



Contents lists available at ScienceDirect

Bioorganic & Medicinal Chemistry

journal homepage: www.elsevier.com/locate/bmc

Preclinical evaluation of a dual sstr2 and integrin $\alpha_v\beta_3$ -targeted heterodimer [^{68}Ga]-NOTA-3PEG₄-TATE-RGD

Bingnan Liu^{a,b}, Zhenzhong Zhang^{c,d}, Hao Wang^{c,d}, Shaobo Yao^{a,*}

^a Department of PET/CT Diagnostic, Department of Hematology, Tianjin Medical University General Hospital, Tianjin 300052, China

^b Department of Hematology, Tianjin Medical University General Hospital, Tianjin 300052, China

^c Department of Nuclear Medicine, Peking Union Medical College Hospital, Chinese Academy of Medical Science & Peking Union Medical College, Beijing 100730, China

^d Beijing Key Laboratory of Molecular Targeted Diagnosis and Therapy in Nuclear Medicine, Beijing 100730, China

ARTICLE INFO

Keywords:

Somatostatin receptor 2

Integrin $\alpha_v\beta_3$

PET

TATE-RGD heterodimer

ABSTRACT

Purpose: Multiple receptors are co-expressed in many types of cancers. Octreotate (TATE) and Arg-Gly-Asp (RGD) peptides target somatostatin receptor 2 (sstr2) and integrin $\alpha_v\beta_3$, respectively. We developed and synthesized a heterodimer NOTA-3PEG₄-TATE-RGD (3PTATE-RGD) and aimed to investigate its characteristics for dual-targeting sstr2 and integrin $\alpha_v\beta_3$.

Methods: TATE and RGD peptides and 1,4,7-triazacyclononane-N',N'',N'''-triacetic acid (NOTA) were linked through a glutamate and polyethylene glycol (PEG) linker, then 3PTATE-RGD was labeled with ^{68}Ga ion. Receptor-binding characteristics and tumor-targeting efficacy were tested *in vitro* and *in vivo* using H69 and A549 lung cancer cell lines and tumor-bearing mice models.

Results: [^{68}Ga]-3PTATE-RGD had comparable sstr2 and integrin $\alpha_v\beta_3$ -binding affinity with monomeric TATE and RGD in cell uptake and PET imaging study, respectively. In the competition study, H69 and A549 tumor uptake of [^{68}Ga]-3PTATE-RGD was completely inhibited in the presence of an excess amount of unlabeled TATE or RGD, respectively. The blocked level didn't grow when both of TATE and RGD mixture was co-injected with [^{68}Ga]-3PTATE-RGD. The pharmacokinetics of [^{68}Ga]-3PTATE-RGD is comparable with [^{68}Ga]-TATE and [^{68}Ga]-RGD, resulting in a larger application.

Conclusion: [^{68}Ga]-3PTATE-RGD showed improved and wider tumor-targeting efficacy compared with monomeric TATE and RGD peptides, which warrants its further investigation in detection both of sstr2 and integrin $\alpha_v\beta_3$ -related carcinomas.

1. Introduction

Lung cancer is the leading cause of cancer-related mortality worldwide. In 2018, the estimated number of new cases of lung and bronchus cancer in the United States is 234,030 and the estimated death is 154,050.¹ Based on the fact, it is crucial to find a precision tool for the diagnosis and therapeutic monitoring of patients with suspected early stage of lung carcinoma.

In the last decades, ^{18}F -FDG positron emission tomography (PET) has become the standard of care in the initial management of patients with lung cancer, especially non-small cell lung carcinoma (NSCLC).² However, false-positive [^{18}F]-FDG PET/CT results in nodal staging have shown in patients with coexistent inflammatory or infectious disease.³ As NSCLC and small cell lung carcinoma (SCLC) are the main histological subtypes and constitutes around 85% and 15% of all lung cancer respectively.⁴ The best method is to find the specific receptors of

protein expressed in each/both of the lung cancer cell lines and then image them using PET. We know that most of NSCLC, including squamous cell carcinoma, large cell carcinoma, adenocarcinoma and other less common types such as pleomorphic, carcinoid tumors, salivary gland carcinoma and unclassified carcinoma and SCLC, have positive expression of integrin receptors. SCLC, including small cell carcinoma (oatcell cancer) and combined small cell carcinoma, belongs to neuroendocrine tumors (NET). Most of NET express high level of somatostatin receptors (sstr) 1–5 at the cell membrane. To be exact, NET express mainly sstr2 and a lower extent sstr5.^{5,6} Based on that theory, precision diagnosis of SCLC or NSCLC using ^{68}Ga labelled TATE or RGD showed good results.^{7–9}

We have been particularly interested in developing a ^{68}Ga -labeled PET tracers due to the favorable properties of ^{68}Ga and dual-targeting capacity for SCLC and NSCLC. As most of lung cancer cell lines express either integrin $\alpha_v\beta_3$ or sstr2, we hypothesized that a peptide ligand

* Correspondence author.

E-mail address: yaoshaobo008@163.com (S. Yao).

<https://doi.org/10.1016/j.bmc.2019.115094>

Received 31 May 2019; Received in revised form 28 August 2019; Accepted 6 September 2019

0968-0896/© 2019 Elsevier Ltd. All rights reserved.

recognizing both receptors would be advantageous over a single receptor-binding tracer.^{10–12} Therefore, in this study, we designed a TATE-RGD heterodimer, in which the cyclic TATE peptide was conjugated with RGD through a glutamate linker. Two representative lung cell lines H69 (sstr2 positive) and A549 (integrin $\alpha_3\beta_3$ positive) were selected.¹³ The *in vitro* biochemical properties including partition coefficients, serum-protein-binding activity, stability assays and cell uptake kinetics assays were performed. *In vivo* tumor-imaging efficacy and biodistribution of [⁶⁸Ga]-3PTATE-RGD were compared with monomeric [⁶⁸Ga]-TATE and [⁶⁸Ga]-RGD counterparts. Specificity and selectivity were also tested.

2. Materials and methods

2.1. General

All chemicals obtained commercially were of analytical grade (Sigma-Aldrich, USA) and used without further purification unless otherwise stated. Solid-phase extraction cartridges (Sep-Pak Plus Light C18 cartridges) was purchased from Waters (MA, USA). Fetal bovine serum (FBS) was purchased from HyClone (Thermo Scientific, USA) and stored below $-20\text{ }^\circ\text{C}$ before use. Millex-GS 0.22 μm filters units were purchased from Merck Millipore Ltd. Reactions were monitored by radio-analytical high performance liquid chromatography (radio-HPLC). We followed the methods of Dr. Yao et al. 2017.¹⁴

2.2. Radiochemistry

NOTA-3PEG₄-TATE-RGD (3PTATE-RGD) were custom manufactured by CS Bio Co (CA, USA). DOTA-TATE (TATE) and NODAGA-RGD (RGD) was purchased from ABX (Germany) (Fig. 1). Radiolabeling procedure was performed manually in a hot cell immediately before injection. Briefly, 1 mL ⁶⁸GaCl₃ eluent (370–555 MBq) obtained from a ⁶⁸Ge/⁶⁸Ga generator (Eckert & Ziegler, Germany) in a 1.5 mL eppendorf

tube was added 93 μL 1.25 mol/L sodium acetate (NaOAc) to adjust the pH range from 4.0 to 4.5. After addition of an aliquot of precursors (30 μg 3PTATE-RGD, 15 μg TATE or 10 μg RGD, 1 $\mu\text{g}/\mu\text{L}$ in water), the reaction tube was incubated at $100\text{ }^\circ\text{C}$ for 10 min. After cooling to room temperature, the reaction mixture was diluted to 5 mL water purified by a Sep-Pak C18 Plus Light Cartridge (preconditioned with 10 mL ethanol and 10 mL water in advance). The C18 cartridge was further washed by water (0.5 mL \times 2) to remove the excess ⁶⁸Ga ion and other water soluble materials, then the radioactivity was eluted with 0.5 mL 75% ethanol. Finally, the purified product [⁶⁸Ga]-3PTATE-RGD, [⁶⁸Ga]-TATE and [⁶⁸Ga]-RGD were diluted in saline and passed through a Millipore filter (0.22 μm , 25 mm) into a sterile product vial.

The HPLC for the radiochemical reaction was equipped with a gamma ray radio detector and a UV detector (Waters system: Waters C18 column, 4.6 \times 250 mm; flow rate: 1 mL/min; mobile phase: 0.01% trifluoroacetic acid (TFA) in water and acetonitrile (CH₃CN); gradient: 0–5 min, 5% CH₃CN; 5–10 min 5%–80% CH₃CN; 15–18 min 80%–100% CH₃CN; 18–20 min 100%–5% CH₃CN.

2.3. Partition coefficient determination

Octanol-water partition coefficient for [⁶⁸Ga]-3PTATE-RGD was determined by measuring the distribution of radiolabeled compound in *n*-octanol and phosphate-buffer saline (PBS, pH = 7.4). A 20 μL sample of [⁶⁸Ga]-3PTATE-RGD (20 μCi) in saline was added to the Eppendorf tube containing 0.5 mL each of *n*-octanol and PBS. After being stirred in a vortex mixture for 10 min, the vial was centrifuged (8000 rpm, 3 min) for layers separation. An aliquot the aqueous and the octanol layer were collected and measured by a γ -counter. $\log P$ values were calculated using the following formula: $\log_{10} P = \log_{10} (\text{counts of } n\text{-octanol} / \text{counts of PBS, mean of } n = 3)$ [10].

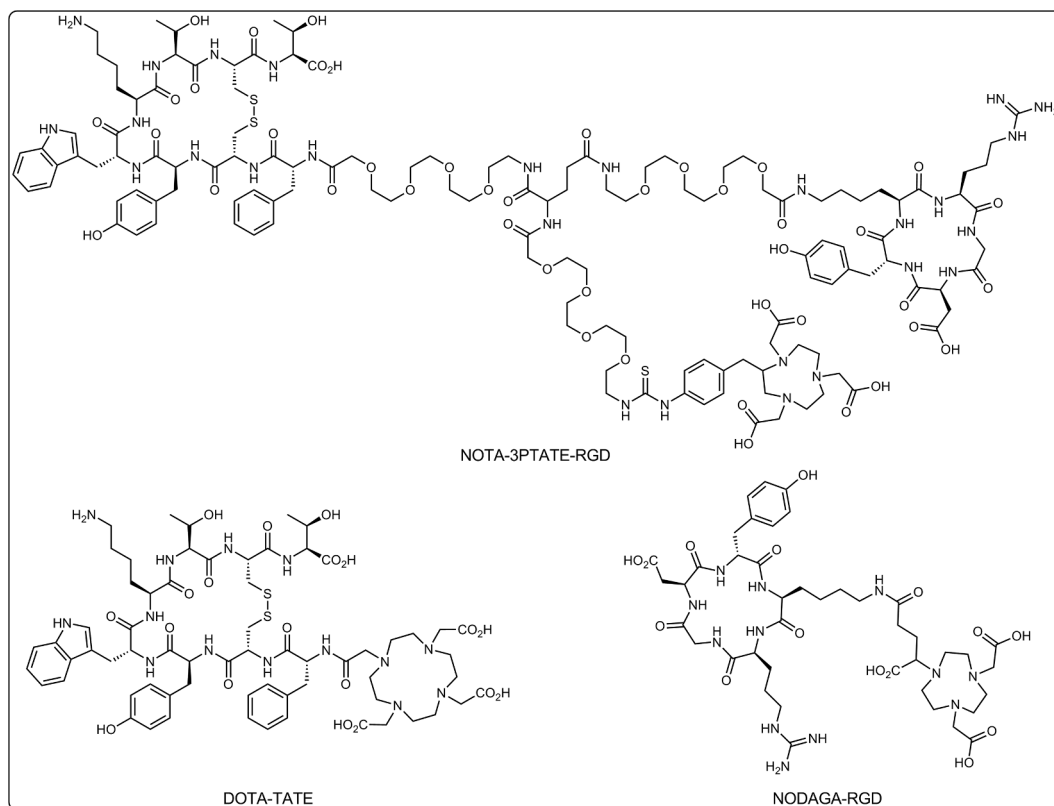


Fig. 1. Schematic structure of NOTA-3PEG₄-TATE-RGD, DOTA-TATE and NODAGA-RGD.

Table 1
Biodistribution of [⁶⁸Ga]-3PTATE-RGD in H69 tumor-bearing nude mice.

Organ	10 min	60 min	120 min
Blood	4.33 ± 0.91	0.88 ± 0.22	0.35 ± 0.10
Brain	0.11 ± 0.04	0.06 ± 0.01	0.04 ± 0.01
Heart	2.24 ± 0.50	0.74 ± 0.11	0.41 ± 0.21
Lung	4.17 ± 1.47	2.25 ± 0.13	1.88 ± 0.04
Liver	2.79 ± 0.50	1.78 ± 0.69	1.12 ± 0.33
Pancreas	2.81 ± 0.52	2.16 ± 0.38	1.94 ± 0.38
Kidney	45.4 ± 2.17	51.6 ± 7.43	47.9 ± 8.70
Spleen	3.89 ± 2.39	1.73 ± 0.17	1.45 ± 0.48
Intestine	1.87 ± 0.27	1.39 ± 0.06	1.08 ± 0.62
Muscle	0.85 ± 0.41	0.38 ± 0.15	0.22 ± 0.03
Stomach	4.68 ± 1.01	4.93 ± 1.26	2.76 ± 0.73
Bone	1.38 ± 0.41	0.71 ± 0.07	0.32 ± 0.13
Tumor	11.4 ± 2.89	12.9 ± 4.52	6.70 ± 1.88

Note: Data are mean % ID/g ± SD (n = 5).

2.4. Protein binding

Protein-bound activity was determined using the following method: The radiolabeled peptide was incubated in fresh human serum at 37 °C and analyzed after 30, 60 and 120 min by size-exclusion chromatography (MicroSpin™ G-50 Columns; Sephadex G-50). Protein binding of [⁶⁸Ga]-3PTATE-RGD was determined by measuring the activity remaining on the column and the activity in the eluent using a γ-counter.

2.5. Cell lines and animal models

Animal experiments were performed in adherence with the Peking Union Medical College Hospital (PUMCH) guidelines for the use of laboratory animals and were approved by PUMCH Clinical Center Animal Care and Use Committee. The human SCLC H69 and NSCLC A549 lung cancer cells were purchased from National Infrastructure of Cell Line Resource. The lung carcinoma tumor-bearing models were generated by subcutaneous injection of 5 × 10⁶ human SCLC H69 and NSCLC A549 cancer cells into the right shoulder of female athymic nude mice (Laboratory Animal Center of PUMCH). Tumor sizes were monitored with a vernier caliper. When the tumor reached approximately 3–5 mm in diameter those tumor-bearing mice were selected and used as a model for imaging.

2.6. In vitro cell binding assays

In the cellular uptake kinetic study, H69 and A549 cells (2 × 10⁵) were seeded into 24-well plates. On the next day, triplicate samples containing approximately 11.1 kBq of [⁶⁸Ga]-3PTATE-RGD, [⁶⁸Ga]-TATE and [⁶⁸Ga]-RGD were added and the cells were incubated at 37 °C for 15, 30, 60 and 120 min. Cells were then washed three times with cold PBS (containing 10% FBS avoiding unspecific binding) and lysed with NaOH (1 mol/L). The cell solution was collected and measured by a γ-counter. The cell uptake was expressed as the percent added dose (% AD) after decay correction.

2.7. In vivo and in vitro stability

For *in vivo* stability tests, balb/c mice were injected intravenously with a dosage of 18.5 MBq (500 μCi) of [⁶⁸Ga]-3PTATE-RGD in 0.2 mL sterile saline. Urine and blood samples were collected at 20 min post-injection and blood was centrifuged (8000 rpm, 10 min) to separate out the plasma. Urine and plasma samples were analyzed by radio-HPLC.

For *in vitro* assays, samples of [⁶⁸Ga]-3PTATE-RGD 0.1 mL (1.85 MBq, 50 μCi) dissolved in sterile saline were incubated with 0.2 mL of fetal bovine serum at 37 °C with gentle shaking. An aliquot of the serum sample was analyzed using radio-HPLC to determine the percentage of intact [⁶⁸Ga]-3PTATE-RGD 120 min post-injection.

2.8. Small-animal PET studies

In vivo PET imaging experiments were using Inveon small-animal PET (micro-PET) scanner (Siemens). Female nude mice bearing H69 and A549 tumors were imaged by micro-PET using [⁶⁸Ga]-3PTATE-RGD, [⁶⁸Ga]-TATE and [⁶⁸Ga]-RGD. For the receptor-blocking experiments, RGD (10 mg/kg), TATE (15 mg/kg), or RGD (10 mg/kg) + TATE (15 mg/kg) were co-injected with [⁶⁸Ga]-3PTATE-RGD injection into H69 (Fig. 3) and A549 (Fig. 4) tumor models via the tail vein. As to the typical imaging process, intravenous injection of 0.2 mL saline (100–200 μCi) was followed by PET scan. Mice were anesthetized with isoflurane and placed on a heating pad to warm the animal throughout the scanning. A ten-minute static PET images were acquired at 30 min postinjection. After the scan, regions of interests (ROIs), including tumor, muscle, brain and kidney were drawn over major organs on decay-corrected whole-body coronal images using Inveon Research Workplace 4.1 software. Radioactivity concentration of organs was obtained from the mean pixel values within the multiple ROI volume, which was converted into MBq/mL using a conversion factor. Assuming the density of tissue was 1 g/cm³, the ROIs were converted to MBq/g and then divided by the administered activity to obtain an imaging ROI-derived %ID/g.

2.9. Ex vivo biodistribution

For the biodistribution study, [⁶⁸Ga]-3PTATE-RGD (1.48–2.96 MBq, 40–80 μCi) in 0.2 mL sterile saline was administrated to adult female H69 and A549 xenografted tumor models (5 per group). At 10, 60 and 120 min postinjection, mice were sacrificed by humane euthanasia, cervical dislocation. Blood was obtained through the eyeball, tissues and organs of interests (brain, heart, lung, liver, pancreas, kidney, spleen, intestine, muscle, stomach, bone and tumor) were weighted and counted. All measurements were background-subtracted and decay-corrected to the time of killing and then averaged. Radioactivity value were calculated and presented as the percentage injected dose per gram (%ID/g) of tissue (Tables 1 and 2).

2.10. Immunostaining and western blot

The tumor status (H69 and A549) was further confirmed by the immunohistochemical (IHC) staining. All the tissue sampling procedure were performed according to the corresponding protocols. Paraffin embedded tumor tissues was sectioned at 5 μm and laid over glass slides and stained for anti-sstr 2 antibody (1:100 Abcam ab78289) and anti-Integrin α_vβ₃ (1:200 Abcam ab134152) followed by secondary antibody with DAKO. The embedded tumor tissues were imaged at 100 × using a Leica DM5000 microscope. Western blot was performed on the H69 and A549 tumor cells to detect sstr2 and integrin α_vβ₃ expression. Briefly,

Table 2
Biodistribution of [⁶⁸Ga]-3PTATE-RGD in A549 tumor-bearing nude mice.

Organ	10 min	60 min	120 min
Blood	4.81 ± 0.60	0.72 ± 0.16	0.40 ± 0.09
Brain	0.29 ± 0.09	0.08 ± 0.01	0.04 ± 0.03
Heart	2.82 ± 0.47	0.75 ± 0.12	0.56 ± 0.09
Lung	6.28 ± 0.69	3.37 ± 0.49	2.27 ± 1.13
Liver	3.67 ± 0.14	2.43 ± 0.60	1.86 ± 0.29
Pancreas	5.65 ± 0.49	4.48 ± 0.27	4.14 ± 0.21
Kidney	45.4 ± 6.00	40.6 ± 16.8	33.2 ± 8.49
Spleen	2.55 ± 0.36	1.83 ± 0.78	1.60 ± 0.66
Intestine	2.90 ± 0.48	1.99 ± 0.21	1.67 ± 0.49
Muscle	1.95 ± 0.12	0.55 ± 0.15	0.49 ± 0.31
Stomach	6.11 ± 0.84	5.54 ± 0.39	5.34 ± 1.85
Bone	1.51 ± 0.47	1.60 ± 0.81	0.71 ± 0.20
Tumor	5.76 ± 1.62	3.40 ± 0.92	2.91 ± 0.78

Note: Data are mean % ID/g ± SD (n = 5).

50 μg of protein lysate was separated by SDS-PAGE and transferred to a PVDF membrane. The membranes were incubated with monoclonal antibodies against sstr2 (1:1000), integrin $\alpha_v\beta_3$ (1:1000) and β -actin (1:1000, Wuhan Goodbio technology CO., LTD), and were detected using an enhanced ECL system (Wuhan Goodbio technology CO., LTD).

2.11. Statistical analysis

Quantitative data were expressed as mean \pm SD. Statistical analysis was performed using the Student's *t*-test (SPSS 19.0). Differences with *P* values of less than 0.05 were considered to be statistically significant.

3. Results

3.1. Radiosynthesis

The radiosynthesis of ^{68}Ga -labeled probe was finished in 20 min with the overall uncorrected radiochemical yield (RCY) of $80 \pm 5\%$ (^{68}Ga]-3PTATE-RGD), $70 \pm 2\%$ (^{68}Ga]-TATE) and $78 \pm 3\%$ (^{68}Ga]-RGD) ($n = 10$, non-decay corrected, n.d.c.). The specific activity (SA) was $> 370 \pm 56 \text{ GBq}/\mu\text{mol}$, $247 \pm 39 \text{ GBq}/\mu\text{mol}$ and $314 \pm 44 \text{ GBq}/\mu\text{mol}$ ($n = 10$), respectively. The radiochemical purity (RCP) was greater than 99% as analyzed by radio-HPLC. The retention time (RT) was 11.7, 11.6 and 10.9 min for ^{68}Ga]-3PTATE-RGD (Fig. 2A), ^{68}Ga]-TATE (Fig. 2B) and ^{68}Ga]-RGD (Fig. 2C).

3.2. In vitro characterization

The partition coefficients ($\log P$) of ^{68}Ga]-3PTATE-RGD was -2.76 ± 0.03 ($n = 3$) indicating high hydrophilicity, a little higher than ^{68}Ga]-NODAGA-RGD ($\log P = -3.6$).¹⁵

Serum-protein-bound activity of ^{68}Ga]-3PTATE-RGD was approximate 25% at 30 min and kept to 120 min. The low affinity to the protein in blood might also be proved by the low ^{68}Ga]-3PTATE-RGD retention in blood which allowed its fast clearance from the blood circulatory system.

Incubation of the tracers in FBS showed high stability *in vitro*. For the *in vivo* stability test in plasma and urine 20 min post-injection, both had only one main peak on radio-HPLC analysis. And the percentage of intact ^{68}Ga]-3PTATE-RGD was greater than 97% (Fig. 2D & E). *In vitro* HPLC analysis of the peptide fraction showed that after 120 min incubation in FBS, more than 97% intact ^{68}Ga]-3PTATE-RGD was found (Fig. 2F).

The cell uptake kinetics of ^{68}Ga]-3PTATE-RGD and its cellular distribution are depicted in Fig. 3. ^{68}Ga]-3PTATE-RGD showed a time-dependent accumulation in H69 and A549 cells. Due to the low receptor-binding affinity of the monomeric RGD peptides and low integrin receptor density in H69 cells, ^{68}Ga]-RGD showed a low cell uptake ($< 1.3\%$ per 10^6 cells). On the other hand, H69 express a high level of sstr2. ^{68}Ga]-TATE binding to sstr2 facilitates effective binding of this radiotracer and the uptake of ^{68}Ga]-TATE is thus rapid and high, reaching about 5% within 30 min of incubation. And the uptake kept to 120 min (Fig. 3A). On the contrary, high integrin expression and low density of sstr2 of A549 cells resulted in a fast and high uptake of ^{68}Ga]-RGD (about 3.5% within 30 min after incubation) and low ^{68}Ga]-TATE uptake ($< 0.9\%$, Fig. 3B). The cell uptake behavior of ^{68}Ga]-3PTATE-RGD is similar to that of ^{68}Ga]-TATE in H69 cells and ^{68}Ga]-RGD in A549 cells, but the uptake value is slightly lower, which might be due to the larger molecular size and other functional group.

3.3. MicroPET imaging

Representative PET images was obtained in H69 (sstr2 positive) and

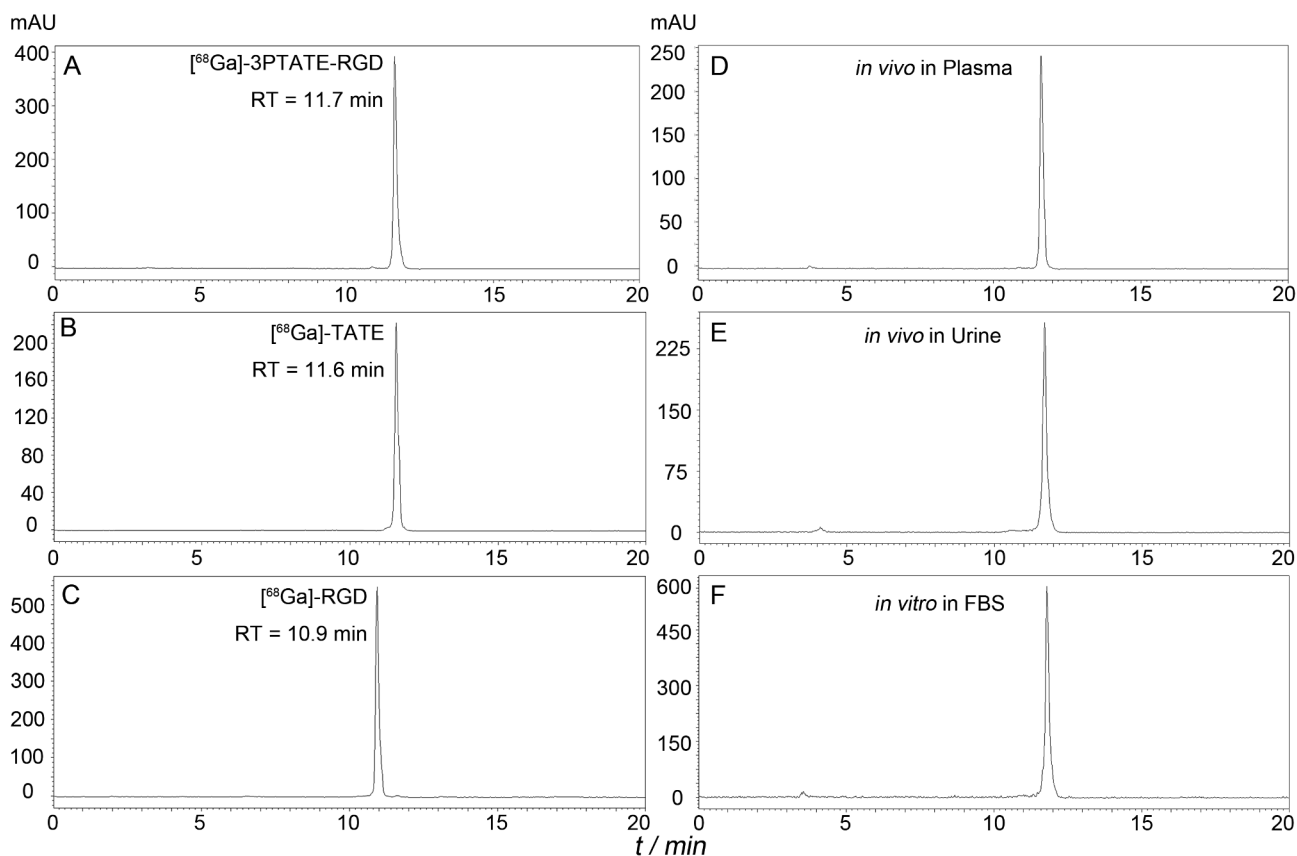


Fig. 2. Radio-HPLC analysis of ^{68}Ga]-3PTATE-RGD (A), ^{68}Ga]-TATE (B) and ^{68}Ga]-RGD (C). *In vivo* stability evaluation of ^{68}Ga]-3PTATE-RGD in plasma (D) and urine (E) 20 min post-injection. *In vitro* stability analysis of ^{68}Ga]-3PTATE-RGD in FBS incubated at 37°C for 120 min (F).

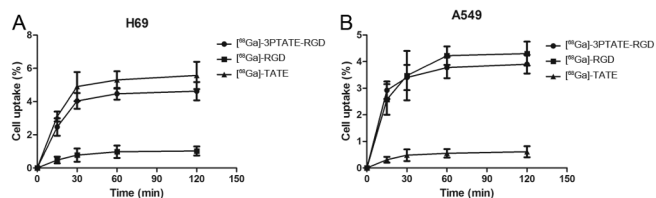


Fig. 3. *In vitro* cellular uptake of [^{68}Ga]-3PTATE-RGD, [^{68}Ga]-TATE and [^{68}Ga]-RGD in H69 (A) and A549 (B) cell lines ($n = 3$, mean \pm SD).

A549 (integrin $\alpha_v\beta_3$ positive) tumor-bearing mice ($n = 4$ per group) after intravenous injection of [^{68}Ga]-3PTATE-RGD, [^{68}Ga]-TATE and [^{68}Ga]-RGD. Predominant urinary excretion of [^{68}Ga]-3PTATE-RGD was represented by the high focal activity concentration in the kidney and urinary bladder.

For the H69 tumor-bearing mice, the xenografted tumors were clearly delineated within 30 min after injection of [^{68}Ga]-3PTATE-RGD (9.78 ± 2.77 %ID/g) and [^{68}Ga]-TATE (10.8 ± 2.63 %ID/g, $P > 0.05$), however, no obvious accumulation of [^{68}Ga]-RGD (2.47 ± 0.21 %ID/g, $P < 0.05$) could be observed (Fig. 4A). For the A549 tumor-bearing mice, the tumors were clearly delineated within 30 min after injection of [^{68}Ga]-3PTATE-RGD (6.46 ± 0.59 %ID/g) and [^{68}Ga]-RGD (5.80 ± 1.63 %ID/g, $P > 0.05$), however, no obvious accumulation of [^{68}Ga]-TATE (2.23 ± 0.55 %ID/g, $P < 0.01$) could be detected (Fig. 5A). The uptake value of tumor, muscle, brain, liver and blood and the ratio of target (tumor) to non-target (N/NT) were summarized in Fig. 4B&C and Fig. 5B&C.

To visualize the extent of receptor-specific (sstr2 and integrin $\alpha_v\beta_3$) uptake of [^{68}Ga]-3PTATE-RGD, *in vivo* competition studies were also performed. Illustrated in Figs. 4D and 5D are the representative images of H69 and A549 tumor-bearing nude mice at 30 min postinjection of [^{68}Ga]-3PTATE-RGD when co-injected with RGD, TATE or RGD + TATE mixture. Tumor uptake of [^{68}Ga]-3PTATE-RGD in control and blocking conditions were summarized in Figs. 4E and 5E.

H69 tumor uptake of [^{68}Ga]-3PTATE-RGD decreased from

9.78 ± 2.77 to 8.23 ± 1.08 ($P > 0.05$) and 1.41 ± 0.73 ($P < 0.01$) %ID/g in presence of RGD or TATE, respectively. A549 tumor uptake decreased from 6.46 ± 0.59 to 1.75 ± 0.53 ($P < 0.001$) and 5.72 ± 0.43 ($P > 0.05$) %ID/g in presence of RGD or TATE, respectively. In addition, when co-injected with RGD + TATE mixture, H69 and A549 tumor uptake values decreased to 1.05 ± 0.13 (Fig. 4E) and 1.35 ± 0.26 %ID/g (Fig. 5E), respectively. However, there is no significant difference in tumor uptake between single peptide (TATE or RGD) and dual peptides (TATE + RGD) blocking, 1.41 ± 0.73 vs. 1.05 ± 0.13 ($P > 0.05$) for H69 and 1.75 ± 0.53 vs. 1.35 ± 0.26 ($P > 0.05$) %ID/g for A549.

3.4. Biodistribution studies

The highest uptake level of [^{68}Ga]-3PTATE-RGD was found in kidneys ($> 40\%$ ID/g at 1 h postinjection), the radioactivity uptake levels of liver and intestine (< 2.5 %ID/g at 1 h) were significantly lower, indicating the predominance of renal excretion route (Tables 1 and 2). Tumors had a high uptake of [^{68}Ga]-3PTATE-RGD at 10 min (11.4 ± 2.89 and 5.76 ± 1.62 %ID/g for H69 and A549 tumor-bearing mice) and declined gradually. Low blood and heart uptake indicated low serum-protein-bound activity which was in accordance to the protein binding study result.

3.5. Immunostaining and western blot

Paraffin wax embedded sections from H69 and A549 tumors, dissected from a mouse that had previously undergone microPET, were cut and stained for immunostaining of sstr2 and integrin $\alpha_v\beta_3$. The tumor section slices were incubated with anti-sstr2 antibody and anti-integrin $\alpha_v\beta_3$, respectively. The staining results were sstr2 (+) and integrin $\alpha_v\beta_3$ (-) in H69 tumors (Fig. 6A&C), sstr2 (-) and integrin $\alpha_v\beta_3$ (+) in A549 tumors (Fig. 6B&D). Both of the staining was found in the membrane of tumor cells. This finding was further corroborated by western blot assays, which indicated overexpression of sstr2 in H69 cells and integrin $\alpha_v\beta_3$ in A549 cells (Fig. 6E).

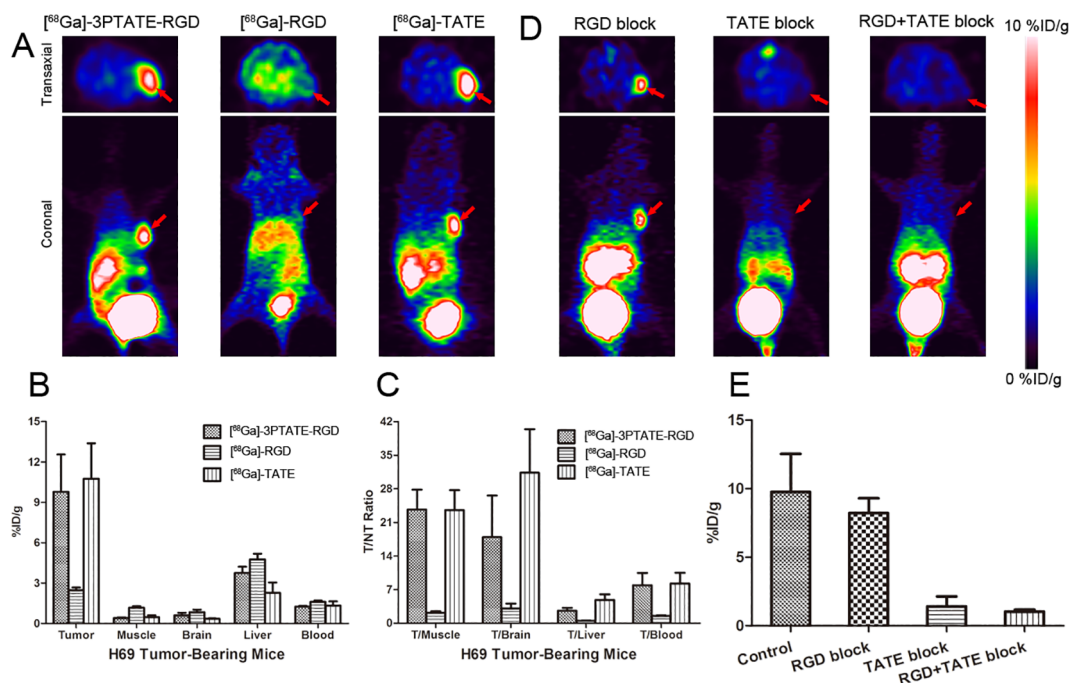


Fig. 4. A: Representative PET images of H69 tumor-bearing mice 30 min after injection of [^{68}Ga]-3PTATE-RGD, [^{68}Ga]-TATE and [^{68}Ga]-RGD. Columns show radioactivity concentration in tumor and other different organs (B) and tumor-to-organ ratios (C). D: Competition PET images 30 min after co-injection of RGD (10 mg/kg), TATE (15 mg/kg) and RGD + TATE. E: Tumor uptake of [^{68}Ga]-3PTATE-RGD in control and blocking studies were summarized. Note: Data are mean % ID/g \pm SD ($n = 4$). (Tumors are marked by red arrows).

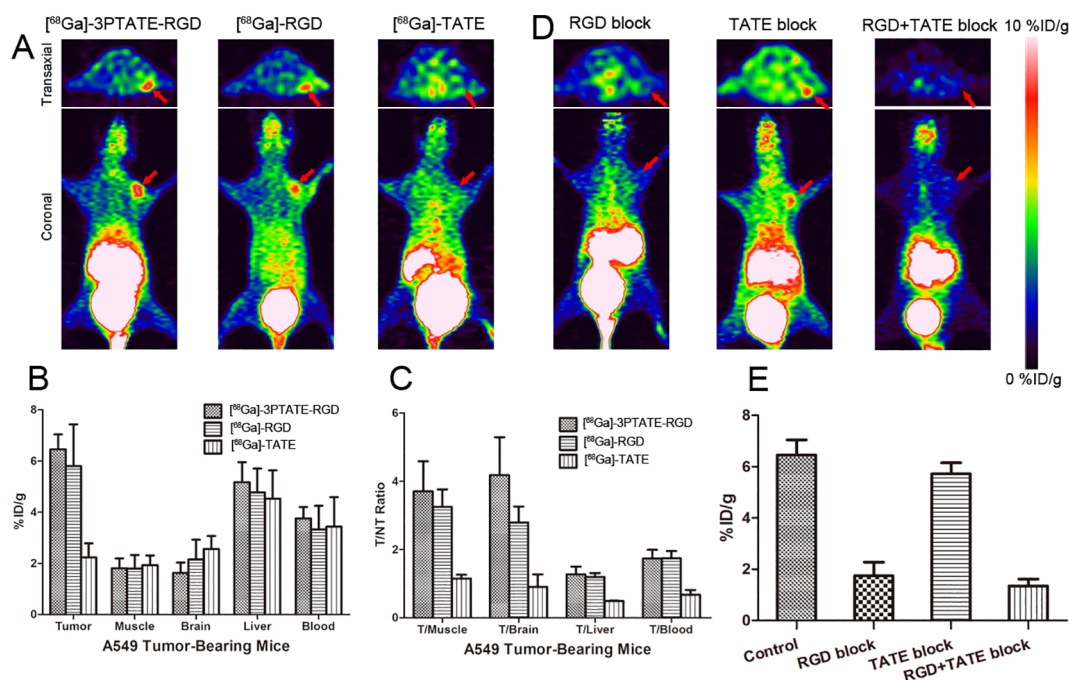


Fig. 5. A: Representative PET images of A549 tumor-bearing mice 30 min after injection of [^{68}Ga]-3PTATE-RGD, [^{68}Ga]-TATE and [^{68}Ga]-RGD. Columns show the radioactivity concentration in tumor and in different organs (B) and tumor-to-organ ratios (C). D: Competition PET images 30 min after co-injection of RGD, TATE and RGD + TATE (10–15 mg/kg). E: Tumor uptake of radioactivity were summarized. Note: Data are mean %ID/g \pm SD ($n = 4$). (Tumors are marked by red arrows).

4. Discussion

The development of radiolabeled peptides for diagnostic and therapeutic applications has expanded exponentially in the last decade.^{16–21} Radiolabeled peptide have many favorable properties, including its fast clearance, rapid penetration, low antigenicity and can be easily produced.^{10,22,23} ^{68}Ga -labeled peptides has attracted considerable interest for cancer imaging because of its physicochemical characteristics²⁴. The ^{68}Ga production is available from an in-house $^{68}\text{Ge}/^{68}\text{Ga}$ generator (^{68}Ge , $t_{1/2} = 270.8$ d), which renders it independent of an onsite cyclotron. With a half-life of 68 min, it is also suitable for the pharmacokinetics of peptidic radiopharmaceuticals. For instance, ^{68}Ga -labeled TATE peptides have been reported to be successful for *ssr2*-positive imaging.^{25,26} ^{68}Ga -labeled RGD peptides were also tested for the imaging of integrin $\alpha_v\beta_3$ -expressing tumors.^{19,27–29} However, the tumor uptake of these tracers were suboptimal owing to the single and relatively low binding affinity of this monomeric peptide and the imperfect

pharmacokinetics.

According to the pathologic type, lung carcinomas can be mainly divided into two categories-SCLC and NSCLC, and each has expression of specific receptors, with high *ssr2*-expressing in SCLC (H69 cell) and high integrin $\alpha_v\beta_3$ -expressing in NSCLC (A549 cells).³⁰ As a result, how to detect both of the two types of lung carcinomas in one PET imaging procedure is our aim. That will save one exposure to radiation from CT and radiotracers. In other words, we wanted to test whether the dual *ssr2* and integrin $\alpha_v\beta_3$ -targeting approach would allow us to develop significantly improved imaging probes over those that recognize only one receptor type.

In this study, we designed and synthesized a dual-target heterodimer NOTA-3PEG₄-TATE-RGD including cyclic RGD, TATE peptides and NOTA, and conjugated them together with PEG₄ chains and glutamate linker (Fig. 1). The reason why we choose NOTA as chelating group is that although DOTA is more widely used as bifunctional chelating agent, it is evident that NOTA is more suitable for complex

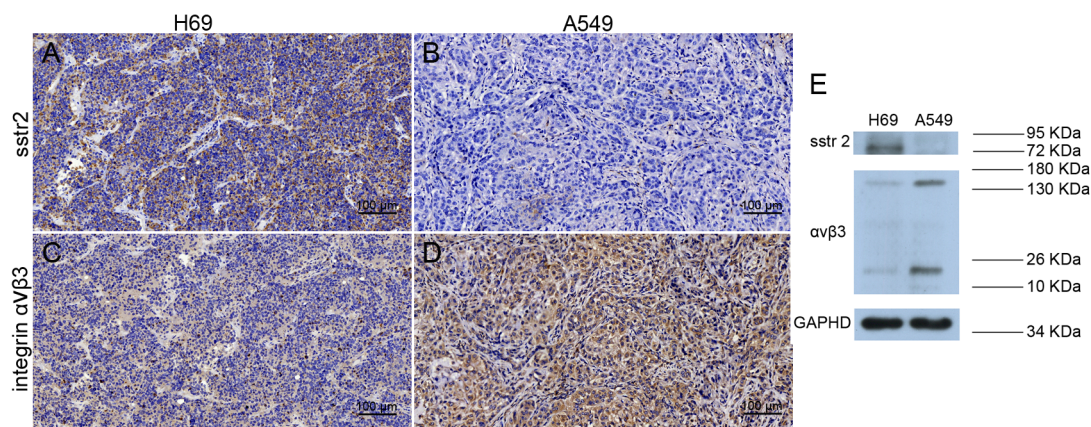


Fig. 6. IHC staining of *ssr2* in H69 (A) and A549 (B) tumor tissue slices and of integrin $\alpha_v\beta_3$ in H69 (C) and A549 (D) tumor tissue slices. Western blot assays of *ssr2* and integrin $\alpha_v\beta_3$ in H69 and A549 tumor cells (E).

formation with Cu^{2+} and Ga^{3+} , which have relatively small ionic diameters than In^{3+} and Y^{3+} (the latter 2 form stable complexes with DOTA).²⁷ 3PTATE-RGD was then labeled with ^{68}Ga for quantitative PET imaging studies. We chose 100 °C and 10 min as the chelating condition because of the high levels of stability of gallium and NOTA complex, and also for the high RCY.

After analyzing the structure of 3PTATE-RGD heterodimer, the peptide is expected to bind both of sstr2 and integrin $\alpha_v\beta_3$ receptors, as the glutamate-PEG linker is supposed to be long enough to allow simultaneous sstr2 and integrin $\alpha_v\beta_3$ binding. The cell-binding study data demonstrated that binding ability of 3PTATE-RGD is similar to TATE for sstr2 binding and is similar to RGD for integrin $\alpha_v\beta_3$. Baseline accumulation of [^{68}Ga]-RGD in H69 and [^{68}Ga]-TATE in A549 cells indicated no expression of integrin $\alpha_v\beta_3$ or sstr2, respectively. Which was approved by IHC staining result (Fig. 6). Another advantage of 3PTATE-RGD over monomeric TATE or RGD is not only the dual-targeting ability, but also the increased number of receptors for signal amplification. Assuming that both of integrin $\alpha_v\beta_3$ or sstr2 receptors have positive expression in one cell line, the ligand binds to sstr2 through TATE moiety, the remaining RGD moiety is able to recognize and bind with integrin $\alpha_v\beta_3$ in close vicinity. The design of heterodimer with a flexible PEG sequence with no receptor binding is for this purpose. Another aim of PEG sequence was to improve the probe's hydrophilicity and metabolism velocity *in vivo*. However, additional experiments using both sstr2 and integrin $\alpha_v\beta_3$ positive expression cell lines are needed to confirm this statement in the future.

In the metabolic stability assays, [^{68}Ga]-3PTATE-RGD showed good stability towards proteinases and metabolic enzyme both *in vitro* and *in vivo*. As cyclic peptide TATE and RGD are also stable *in vivo*. In the partition coefficients study, high hydrophilicity of [^{68}Ga]-3PTATE-RGD ($\log P = -2.76 \pm 0.03$, $n = 3$) predicating the tracer might be metabolized and excreted through the urinary-bladder system. The prediction was proved by the *ex vivo* biodistribution and PET study, as the high radioactivity uptake in kidney and bladder and low accumulation in liver and gallbladder.

In the cell kinetic study, cell uptake of [^{68}Ga]-3PTATE-RGD was fast and climbed to a high level (around 5%) in 60 min in both of the two cell lines and kept until to the end. Compared to [^{68}Ga]-TATE in H69 and [^{68}Ga]-RGD in A549 cells, [^{68}Ga]-3PTATE-RGD represented a little lower binding ability. However, it did not influenced the imaging quality in PET study, as [^{68}Ga]-3PTATE-RGD showed high T/NT ratio and good images.

The imaging quality of [^{68}Ga]-3PTATE-RGD was tested in the H69 and A549 tumor-bearing model. Our PET assays demonstrated that H69 tumor/muscle ratio of [^{68}Ga]-3PTATE-RGD was similar to [^{68}Ga]-TATE (23.7 ± 4.13 vs. 23.6 ± 4.14 , $P > 0.05$), but much higher than [^{68}Ga]-RGD (2.14 ± 0.35 , $P < 0.001$) (Fig. 4C). In A549 tumors, the tumor/muscle ratio of [^{68}Ga]-3PTATE-RGD was a little better than [^{68}Ga]-RGD (3.71 ± 0.88 vs. 3.25 ± 0.51 , $P > 0.05$), but higher than [^{68}Ga]-TATE (1.15 ± 0.11 , $P < 0.01$) (Fig. 5C). Which means the restructuring of TATE and RGD to a dual-targeted tracer and flexible linker (glutamate and PEG) did not influence the binding ability of single TATE or RGD peptide *in vivo*. The pharmacokinetics was not significantly improved for [^{68}Ga]-3PTATE-RGD compared with [^{68}Ga]-TATE and [^{68}Ga]-RGD. Which may be attributed to the larger molecular size, different charge and hydrophilicity of [^{68}Ga]-3PTATE-RGD. In the present study, high uptake levels in tumors and kidneys predominated in biodistribution and imaging studies in H69 and A549 tumor-bearing nude mice. Although the uptake level in kidneys and bladder was high, it is acceptable for a PET agent because it can be easily kept under a hazardous radiation level and will seldom disturb image-reading or analysis, especially for the lower abdomen.

In the competition experiment, no obvious decreased tumor uptake of [^{68}Ga]-3PTATE-RGD could be observed in presence of RGD in H69 or TATE in A549 tumor (Fig. 4D&5D). Which means that almost no expression of integrin $\alpha_v\beta_3$ in H69 or sstr2 in A549 cells exist. The

prediction was proved by IHC staining. Co-injection of TATE and RGD mixture significantly decreased the tumor uptake meant a total blocking of both integrin $\alpha_v\beta_3$ and sstr2 receptors in H69 and A549 cell lines. However, the blocking level did not grow significantly compared with single peptide-blocking assay.

Both sstr and integrin protein are frequently expressed on the lung carcinomas cell membrane. IHC analysis revealed positive sstr2 expression in H69 cells³¹ and positive integrin $\alpha_v\beta_3$ expression in A549 cells,^{32,33} which are in accordance to the PET imaging results. Western blot experiments further confirmed the specific expression of the sstr2 in H69 and integrin $\alpha_v\beta_3$ in A549 cells (Fig. 6E).

5. Conclusion

In this study, a novel dual sstr2 and integrin $\alpha_v\beta_3$ receptor-targeting heterodimer 3PTATE-RGD was designed, synthesized, labeled with ^{68}Ga and evaluated *in vitro* and *in vivo*. [^{68}Ga]-3PTATE-RGD showed good pharmacokinetics and high T/NT ratio in H69 and A549 tumor-bearing models. As tumors often co-express multiple receptors, this strategy provides a general method of imaging dual receptor expressing carcinomas.

6. Data availability

The data included in this study are available upon request from the corresponding author.

Acknowledgement

This study was funded in part by the National Natural Science Foundation of China 81601529, Natural Science Foundation of Tianjin 18JJCQNJC11600, Tianjin Medical University General Hospital Special Fund for Talent Training & New Century Talent Programme, Tianjin Medical University Basic Research Foundation 2018KJ060.

Conflict of interest

The authors declare no conflicts of interest.

Appendix A. Supplementary data

Supplementary data to this article can be found online at <https://doi.org/10.1016/j.bmc.2019.115094>.

References

- National Cancer Institute N, U.S. <https://seer.cancer.gov/statfacts/html/all.html>. 2018. Lung and Bronchus Cancer (Online).
- Chang AJ, Dehdashti F, Bradley JD. The role of positron emission tomography for non-small cell lung cancer. *Pract Radiat Oncol*. 2011;1:282–288.
- Billé A, Pelosi E, Skanjeti A, et al. Preoperative intrathoracic lymph node staging in patients with non-small-cell lung cancer: accuracy of integrated positron emission tomography and computed tomography. *Eur J Cardiothorac Surg*. 2009;36:440–445.
- Garg PK, Singh SK, Prakash G, Jakhettiya A, Pandey D. Role of positron emission tomography-computed tomography in non-small cell lung cancer. *World J Methodol*. 2016;6(1):105–111 26.
- Reubi JC, Schär JC, Waser B, et al. Affinity profiles for human somatostatin receptor subtypes SST1–SST5 of somatostatin radiotracers selected for scintigraphic and radiotherapeutic use. *Eur J Nucl Med*. 2000;27:273–282.
- Hanin FX, Pauwels S, Bol A, Breeman W, de Jong M, Jamar F. Tumor uptake of ^{68}Ga -DOTA-Tyr³-octreotate: animal PET studies of tumor flow and acute somatostatin receptor modulation in the CA20948 rat model. *Nucl Med Biol*. 2010;37:157–165.
- Zheng K, Liang N, Zhang J, et al. ^{68}Ga -NOTA-PRGD₂ PET/CT for Integrin Imaging in Patients with Lung Cancer. *J Nucl Med*. 2015;56:1823–1827.
- Kayani I, Conry BG, Groves AM, et al. A comparison of ^{68}Ga -DOTATATE and ^{18}F -FDG PET/CT in pulmonary neuroendocrine tumors. *J Nucl Med*. 2009;50:1927–1932.
- Lapa C, Hänscheid H, Wild V, et al. Somatostatin receptor expression in small cell lung cancer as a prognostic marker and a target for peptide receptor radionuclide therapy. *Oncotarget*. 2016;7:20033–20040.
- Li ZB, Wu Z, Chen K, Ryu EK, Chen X. ^{18}F -labeled BBN-RGD heterodimer for prostate cancer imaging. *J Nucl Med*. 2008;49:453–461.

11. Liu Z, Yan Y, Chin FT, Wang F, Chen X. Dual integrin and gastrin-releasing peptide receptor targeted tumor imaging using ^{18}F -labeled PEGylated RGD-bombesin heterodimer ^{18}F -FB-PEG₃-Glu-RGD-BBN. *J Med Chem.* 2009;52:425–432.
12. Liu Z, Yan Y, Liu S, Wang F, Chen X. ^{18}F , ^{64}Cu , and ^{68}Ga labeled RGD-bombesin heterodimeric peptides for PET imaging of breast cancer. *Bioconjugate Chem.* 2009;20(5):1016–1025.
13. Santini C, Kuil J, Bunschoten A, et al. Evaluation of a fluorescent and radiolabeled hybrid somatostatin analogue in vitro and in mice bearing H69 neuroendocrine xenografts. *J Nucl Med.* 2016;57:1289–1295.
14. Yao SB, Luo YP, Zhang ZZ, Hu GL, Zhu ZH, Li F. Preclinical PET imaging of HIP/PAP using $1'$ - ^{18}F -fluoroethyl- β -D-lactose. *Oncotarget.* 2017;8:75162–75173.
15. Knetsch PA, Petrik M, Griessinger CM, et al. [^{68}Ga]NODAGA-RGD for imaging $\alpha v \beta 3$ integrin expression. *Eur J Nucl Med Mol Imaging.* 2011;38:1303–1312.
16. Kratochwil C, Giesel FL, Eder M, et al. [^{177}Lu] Lutetium-labelled PSMA ligand-induced remission in a patient with metastatic prostate cancer. *Eur J Nucl Mol Imaging.* 2015;42:987–988.
17. Benešová M, Schäfer M, Bauder-Wüst U, Afshar-Oromieh A, Kratochwil C, et al. Preclinical Evaluation of a Tailor-Made DOTA-Conjugated PSMA Inhibitor with Optimized Linker Moiety for Imaging and Endoradiotherapy of Prostate Cancer. *J Nucl Med.* 2015;56:914–920.
18. Luo Y, Pan Q, Yao S, et al. Glucagon-like Peptide-1 Receptor PET/CT with ^{68}Ga -NOTA-exendin-4 for Detecting, Localized Insulinoma: a Prospective Cohort Study. *J Nucl Med.* 2016;57:715–720.
19. Li ZB, Chen K, Chen XY. ^{68}Ga -labeled multimeric RGD peptides for microPET imaging of integrin $\alpha v \beta 3$ expression. *Eur J Nucl Med Mol Imaging.* 2008;35:1100–1108.
20. Eder M, Schäfer M, Bauder-Wüst U, et al. ^{68}Ga -Complex lipophilicity and the targeting property of a urea-based PSMA inhibitor for PET imaging. *Bioconjugate Chem.* 2012;23:688–697.
21. Zhang J, Niu G, Lang L, et al. Clinical translation of a dual integrin $\alpha_v \beta_3$ and GRPR targeting PET radiotracer ^{68}Ga -NOTA-BBN-RGD. *J Nucl Med.* 2017;58:228–234.
22. Liu S. Radiolabeled multimeric cyclic RGD peptides as integrin $\alpha_v \beta_3$ targeted radiotracers for tumor imaging. *Mol Pharm.* 2006;3:472–487.
23. Benedetti E, Morelli G, Accardo A, Mansi R, Tesaro D, Aloj L. Criteria for the design and biological characterization of radiolabeled peptide-based pharmaceuticals. *Bio Drugs.* 2004;18:279–295.
24. Maecke HR, Hofmann M, Haberkorn U. ^{68}Ga -labeled peptides in tumor imaging. *J Nucl Med.* 2005;46(Suppl 1):172S–178S.
25. Zhang JJ, Zhu ZH, Zhong DR, et al. ^{68}Ga -DOTATATE PET/CT is an Accurate Imaging Modality in the Detection of Culpit Tumors Causing Osteomalacia. *Clin Nucl Med.* 2015;40:642–646.
26. Santini C, Kuil J, Bunschoten A, et al. Evaluation of a Fluorescent and Radiolabeled Hybrid Somatostatin Analog In Vitro and in Mice Bearing H69 Neuroendocrine Xenografts. *J Nucl Med.* 2016;57:1289–1295.
27. Jeong JM, Hong MK, Chang YS, et al. Preparation of a Promising Angiogenesis PET Imaging Agent: ^{68}Ga -Labeled c(RGDyK)-Isothiocyanatobenzyl-1,4,7-Triazacyclononane-1,4,7-Triacetic Acid and Feasibility Studies in Mice. *J Nucl Med.* 2008;49:830–836.
28. Decristoforo C, Gonzalez IH, Carlsen J, et al. ^{68}Ga - and ^{111}In -labelled DOTA-RGD peptides for imaging of $\alpha v \beta 3$ integrin expression. *Eur J Nucl Med Mol Imaging.* 2008;35:1507–1515.
29. Guo N, Lang LX, Li WH, et al. Quantitative Analysis and Comparison Study of [^{18}F]AIFNOTA-PRGD₂, [^{18}F]FPPRGD₂ and [^{68}Ga]Ga-NOTA-PRGD₂ Using a Reference Tissue Model. *PLoS One.* 2012;:e37506.
30. Zhang Y, Yang J, Ding MH, et al. Tumor-penetration and antitumor efficacy of cetuximab are enhanced by co-administered Irgd in a murine model of human NSCLC. *Oncol Lett.* 2016;12:3241–3249.
31. Falcioni R, Cimino L, Gentileschi MP, et al. Expression of beta 1, beta 3, beta 4, and beta 5 integrins by human lung carcinoma cells of different histotypes. *Exp Cell Res.* 1994;210:113–122.
32. Zhou T, Xiao X, Xu B, Li H, Zou Y. Overexpression of sstr2 inhibited the growth of sstr2-positive tumors via multiple signaling pathways. *Acta Oncol.* 2009;48:401–410.
33. Singh SP, Han L, Murali R, et al. sstr2-based reporters for assessing gene transfer into non-small cell lung cancer: evaluation using an intrathoracic mouse model. *Hum Gene Ther.* 2011;22:55–64.